International Journal of Sediment Research 34 (2019) 496–508

Contents lists available at ScienceDirect

International Journal of Sediment Research

journal homepage: www.elsevier.com/locate/ijsrc

Original Research

Turbulence and suspended sediment processes in the Garonne River tidal bore in november 2016

David Reungoat [a,c], Xinqian Leng [b], Hubert Chanson [b,*]

[a] Université de Bordeaux, I2M, Laboratoire TREFLE, 16 Avenue Pey-Berland, Pessac, France
[b] The University of Queensland, School of Civil Engineering, Brisbane, QLD 4072, Australia
[c] CNRS UMR 5295, 33607 Pessac, France

ARTICLE INFO

Article history:
Received 28 June 2018
Received in revised form
27 February 2019
Accepted 19 March 2019
Available online 22 March 2019

Keywords:
Tidal bore
Garonne River
Hydrodynamics
Suspended sediment
Field observations
Turbulence-sediment suspension interactions

ABSTRACT

A tidal bore is a water discontinuity at the leading edge of a flood tide wave in estuaries with a large tidal range and funneling topography. New measurements were done in the Garonne River tidal bore on 14–15 November 2016, at a site previously investigated between 2010 and 2015. The data focused on long, continuous, high-frequency records of instantaneous velocity and suspended sediment concentration (SSC) estimate for several hours during the late ebb, tidal bore passage and flood tide. The bore passage drastically modified the flow field, with very intense turbulent and sediment mixing. This was evidenced with large and rapid fluctuations of both velocity and Reynolds stress, as well as large SSCs during the flood tide. Granulometry data indicated larger grain sizes of suspended sediment in water samples compared to sediment bed material, with a broader distribution, shortly after the tidal bore. The tidal bore induced a sudden suspended sediment flux reversal and a large increase in suspended sediment flux magnitude. The time-variations of turbulent velocity and suspended sediment properties indicated large fluctuations throughout the entire data set. The ratio of integral time scales of SSC to velocity in the x-direction was on average $T_{E,SSC}/T_{E,x} \sim 0.16$ during the late ebb tide, compared to $T_{E,SSC}/T_{E,x} \sim 0.09$ during the late flood tide. The results imply different time scales between turbulent velocities and suspended sediment concentrations.

1. Introduction

A tidal bore is a hydrodynamic discontinuity at the leading edge of a flood tide wave in estuaries with a large tidal range and funneling topography. Bore inception requires a combination of tidal, bathymetric, and riverine conditions for its appearance (Bartsch-Winkler & Lynch, 1988; Chanson, 2011). The driving process is a flood tide with a longitudinal-maximum tidal range larger than 4–5 m, together with its amplification during the upstream propagation (Tricker, 1965). After formation, the bore's leading edge is characterised by an abrupt rise in water surface elevation, which corresponds to a singularity in water depth, pressure, and velocity (Lighthill, 1978).

A tidal bore advancing upstream may scour the river bed and advect suspended sediment materials in its wake, as evidenced in the field (Chanson et al., 2011; Furgerot, 2014; Greb & Archer, 2007). The very-early flood tide flow is characterised by very-high suspended sediment concentrations (Fan et al., 2014; Reungoat et al., 2017a). For example, the Petitcodiac River tidal bore (Canada) was called "a fast moving wall of brown churning water" (Larracey, 1985); in China, the Qiantang River bore can generate "a very turbulent wake region in which the water surface is nearly black" (Keevil et al., 2015); in Brazil, "the water boiled violently after the passage of the bore and became brownish-black" in the Rio Mearim (Kjerfve & Ferreira, 1993). Numerous accounts of tidal bores emphasised the intense sediment load during the early flood tide (Chanson, 2011). Field measurements reported suspended sediment concentration (SSC) levels for which non-Newtonian fluid behaviour might be expected (Keevil et al., 2015; Reungoat et al., 2017a). In natural estuaries, a tidal bore changes its shape with changes in estuarine channel topography, adding complications to the interactions between hydrodynamic and sediment processes. Further numerous observations have highlighted changes in bore shape at the same observation site, from one flood tide to the next.

The Garonne River bore was previously investigated in the Arcins Channel between 2010 and 2015, although for a limited

* Corresponding author.
E-mail address: h.chanson@uq.edu.au (H. Chanson).

https://doi.org/10.1016/j.ijsrc.2019.03.003

time span at each occurrence. Herein, a detailed hydrodynamic and suspended sediment study was done on 14 and 15 November 2016. Two key features were the continuous sampling at high frequency for several hours of both velocity and SSC, as well as detailed measurements of suspended sediment properties before, during, and after the bore. Records included a total of 15 h of high-frequency data around the tidal bore passage, recorded over two consecutive days. The data analysis provides an unique characterisation of rapid time-variations in velocity and suspended sediment properties.

2. Methods

2.1. Study site and instrumentation

Measurements were done in the Arcins Channel, Garonne River, at a location 6 km upstream of Bordeaux (France) (Fig. 1). This site was previously used between 2010 and 2015. Cross-sectional surveys on 14 and 15 November 2016 at the end of the ebb tide are shown in Fig. 2, with z the vertical elevation in m Nivellement Général de la France Institut Géographique National 1969 (NGF IGN69). Field measurements were done under spring tide conditions when the tidal range in Bordeaux was 6.01 m and 6.09 m, respectively (Table 1).

The water surface elevations were sampled manually. During the bore front passage, water level records were measured using a High Definition (HD) video camera (Sony™ HDR PJ200E (25 fps)) and the video data were post-treated manually to ensure high quality data. At other times, the survey staff was read manually every 10 min. Instantaneous velocity component measurements were made with a Nortek™ Acoustic Doppler Velocimeter (ADV) Vectrino+ (10 MHz, serial number VNO1356, firmware version 1.31), sampling continuously at 200 Hz. The start and end times for sampling are listed in Table 1. In Fig. 2B, the ADV sampling volume is shown with its surroundings. The ADV settings were a velocity range of 2.5 m/s, a transmit length of 0.3 mm, a sampling volume of 1.5 mm height, and a sampling rate of 200 Hz. The ADV power setting was High-, to optimise the backscatter response of the ADV system with the river sediment (Reungoat et al., 2017a). The ADV data were post-processed to eliminate any erroneous and corrupted data (Reungoat et al., 2017b). The percentage of good samples was 83% and 87% for the 14 and 15 November 2016 data sets, respectively. Visual observations were recorded with digital single lens reflex (dSLR) cameras and high-definition (HD) digital video cameras (Reungoat et al., 2017b, and Digital Appendix).

2.2. Turbulence characterisation

Turbulent velocity components and acoustic backscatter were sampled at 200 Hz continuously, including during the bore

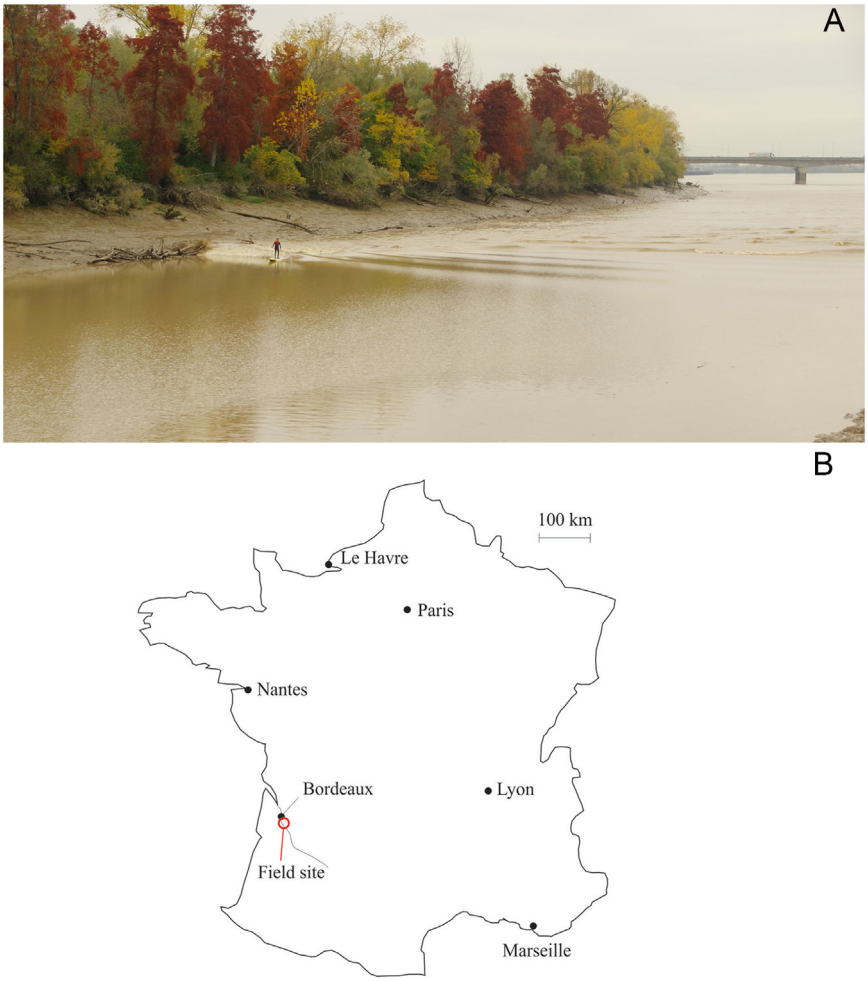

Fig. 1. Tidal bore of the Garonne River in the Arcins Channel on 15 November 2016; (A) Advancing tidal bore in the Arcins Channel - The tidal bore was breaking near the river banks and undular in the central channel section - The Arcins Island is on the left and the sampling site is next to the right bank, with the city of Bordeaux in the background; and (B) Map of France with field site location.

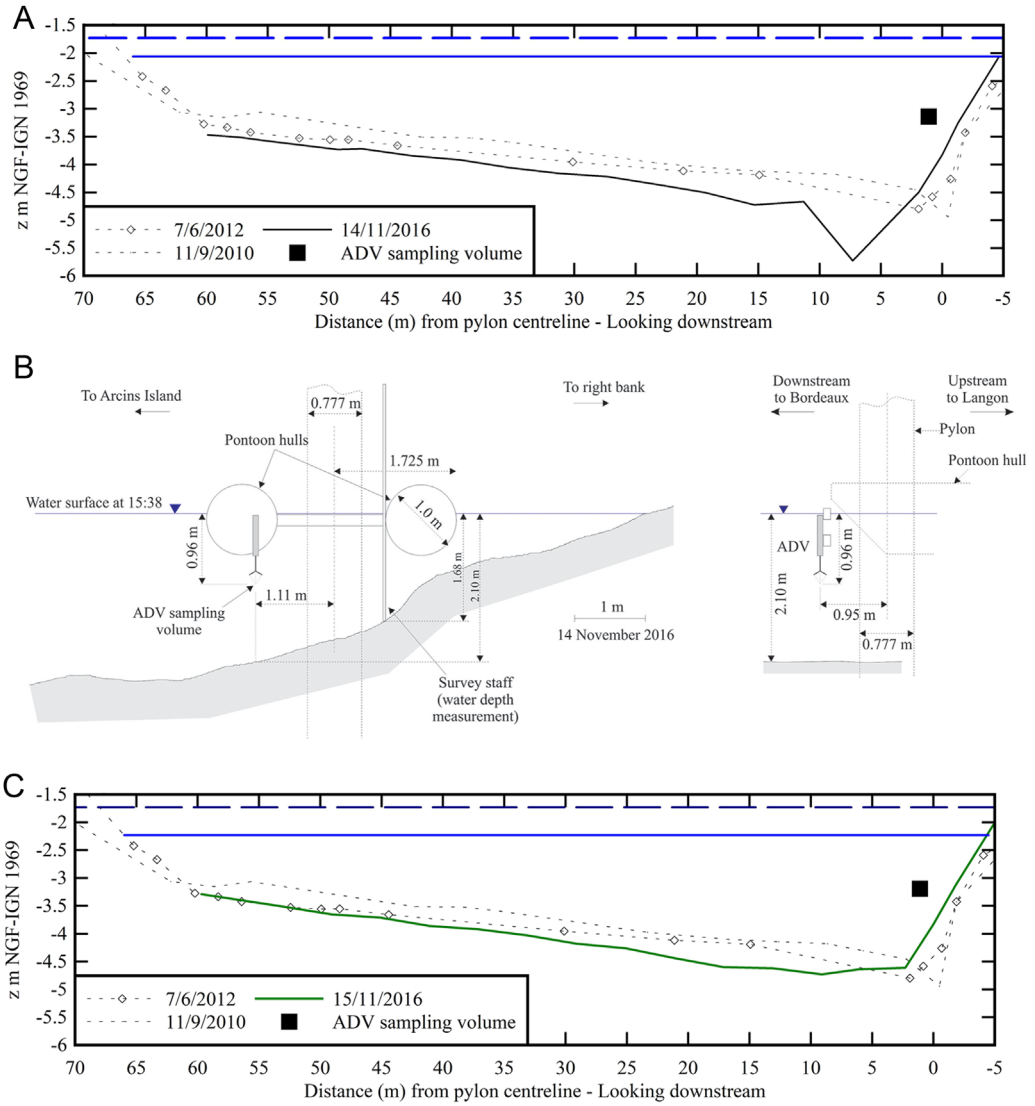

Fig. 2. Surveyed cross-section of the Arcins Channel, Garonne River (France) looking downstream (i.e. north); (A) Surveyed (distorted) cross-sections on 14 November 2016 - Comparison with the 2010 and 2012 survey data at the same cross-section - Water levels immediately before (thick blue solid line) and after (thick dark blue dashed line) the bore front are shown as well as the Acoustic Doppler Velocimeter (ADV) control volume before bore passage (black square); (B) Un-distorted detail drawing of the bed topography, ADV mounting, sampling volume location and water surface 2 min prior to the tidal bore on 14 November 2016 - Left: looking downstream (i.e. North) - Right: view from Arcins Island; and (C) Surveyed (distorted) cross-sections on 15 November 2016 - Same legend as Fig. 2A.

Table 1
Velocity field measurements in the tidal bore of the Garonne River, Arcins Channel (France) in 2016.

Reference	Date	Tidal range (m)	ADV system	Sampling rate (Hz)	Sampling duration	Start time	Tidal bore time	End time	ADV sampling volume location
(1)	(2)	(3)	(4)	(5)	(6)	(7)	(8)	(9)	(10)
Current study	13/11/2016	5.66	Visual observations	N/A	N/A	N/A	14:45	N/A	N/A
	14/11/2016	6.01	Nortek Vectrino+	200	5 h 6 min	12:31	15:43	17:37	About 5.6 m from right bank waterline (at low
	15/11/2016	6.09			8 h 19 min	11:45	16:32	20:04	tide) 0.96 m below water surface. Basically same location as in 2013 and 2015.

Notes: Tidal range: measured at Bordeaux; Start time: starting time of ADV sampling record; End time: end time of ADV sampling record; All times are expressed in local times using the local time zone: e.g., (UTC +1) on 14 and 15 November 2016; N/A: not applicable.

passage. The instantaneous signals were processed using samples containing 10,000 points (50 s), and re-calculated every 10 s along the entire sampling duration. The sample size (10,000 points or 50 s) was selected as substantially longer than the instantaneous velocity fluctuation time scales while containing enough points (10,000) for statistically meaningful outcomes. The selection was derived based upon a sensitivity analysis following (Trevethan et al., 2007; Trevethan et al., 2008). In the current study, the flow was considered quasi-steady over the sample duration (50 s), and the statistical moments were determined by time-averaging. The

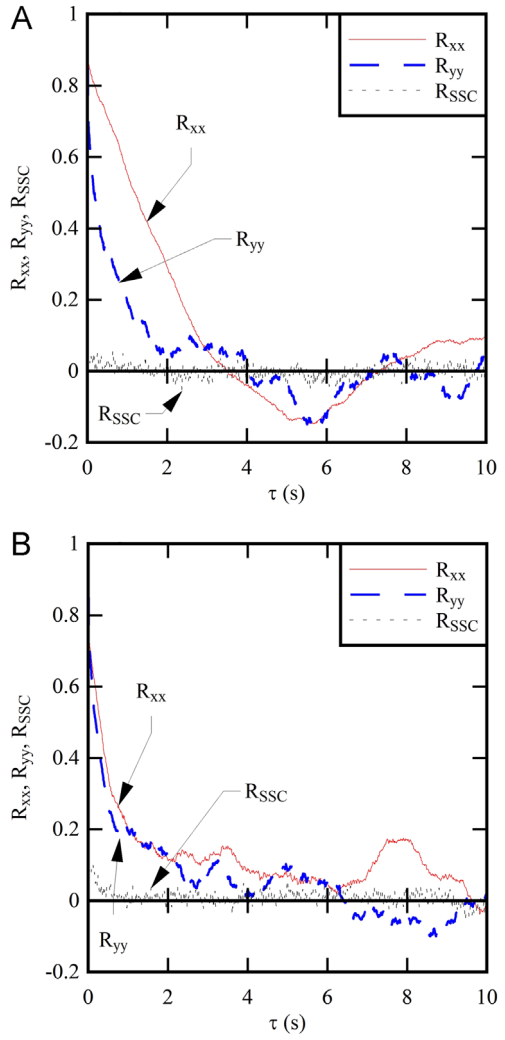

Fig. 3. Auto-correlation functions for the longitudinal and transverse velocity component as well as the suspended sediment concentration about 1 h after the bore passage in the Arcins Channel; (A, Left) 14 November 2016; (B, Right) 15 November 2016 - Calculations done over 10,000 samples.

method was tested to be suitable for gradually-varying unsteady flows, before and after the bore passage.

The characteristic turbulent time scales were calculated in terms of the three velocity components (V_x, V_y, V_z) and suspended sediment concentration (SSC). The integral time scale, $T_{E,i}$, of property i, with i = V_x, V_y, V_z, or SSC, was calculated as:

$$T_{E,i} = \int_{\tau=0}^{\tau(R_{ii}=0)} R_{ii} \times d\tau \quad (1)$$

where τ is the time lag, and R_{ii} is the normalised auto-correlation function of the velocity data of property i calculated as:

$$R_{ii,\tau} = \frac{\int_{t=0}^{T} i(t) \times i(t+\tau) \times dt}{\left(\int_{t=0}^{T} i(t) \times dt\right)^2} \quad (2)$$

in which the integration time, T, must be significantly larger than the integral turbulent time scale, T_E, and smaller than the hydrodynamic time scale. $T_{E,i}$ represents a rough measure of the longest connection in the turbulent behaviour of property i (Bradshaw, 1971; Piquet, 1999).

A sensitivity analysis was done in tidal bore flow for 0.5 < T < 10 s by Chanson and Toi (2015). Little difference was observed with T ≥ 2 s and the current study used T = 50 s. Fig. 3 shows typical auto-correlation function results calculated 1 h after the bore passage.

2.3. Characterisation of sediment materials

Both sediment bed and sediment-laden water samples were collected on each day. The bed material was taken at the end of the ebb tide above the waterline. Bottles were filled with water collected 0.2 m below the water surface on both days, including prior to, during, and after the bore front passage. A series of laboratory tests were subsequently done to measure the sediment particle size distribution, rheometry of bed samples, and backscatter characteristics of suspended sediment solutions.

The granulometry data were measured using a Malvern™ laser Mastersizer 2000 equipped with a Hydro 3000SM dispersion unit for wet samples. The rheological properties were tested with a rheometer Malvern™ Kinexus Pro (Serial MAL1031375) equipped with a plane-cone (Diameter = 40 mm, cone angle: 4°, gap truncation: 150 μm). All tests were done under a controlled strain rate at constant temperature (25 °C).

The calibration of the ADV backscatter signal was done using artificially produced concentrations of sediment bed material, using the same Nortek™ ADV Vectrino+ system with the same settings as during the field measurements. Further discussion on the calibration method can be found in Reungoat et al. (2017b).

2.4. Sediment properties

The relative density of sediment was 2.68 and 1.31 for dry and wet sediment samples, respectively. Both bed and suspended sediment samples consisted of silty cohesive materials. Particle size distribution data are shown in Fig. 4. Fig. 4A shows typical grain size distributions of suspended sediment (thin lines) and bed sediment materials (thick lines). The median particle size was 11.8 μm and 16.8 μm for suspended sediment and bed material, respectively, within the silt size range (Graf, 1971; Julien, 1995). The sorting coefficient was 3.37 and 3.95 for the suspended sediment and bed material, respectively. The measurements suggested a slightly broader range of bed material particle sizes compared to the suspended sediment sizes (Fig. 4A). Overall the data were close to previous observations, between 2012 and 2015 at the same site. The suspended sediment data showed larger and broader grain size distributions shortly after the bore passage (Fig. 4B). This is seen in Fig. 4B showing the characteristic grain sizes as functions of the relative time of passage of tidal bore, t -T_{bore}. The median suspended sediment grain size (d_{50}) was 15% larger after than before the tidal bore, while the d_{10} and d_{90} characteristic sizes were about 20% larger after the bore. All grain size data showed a significant scatter after the bore front, as illustrated in Fig. 4B. The scatter was not a measurement error, but rather reflected the non-homogeneous nature of the suspended load advected behind the tidal bore. For comparison, a more limited data set in October 2015 yielded a median suspended grain size about 40% larger after than before the tidal bore, with the d_{10} and d_{90} characteristic sizes of suspended sediment 60% to 50% larger after the bore passage (Reungoat et al., 2017a).

Instantaneous SSC estimates were deduced from the ADV backscatter signal data. The relation between ADV backscatter amplitude and SSC was calibrated for SSCs between 0 and 90 kg/m^3. Experimental results are summarised in Fig. 5: a monotonic increase in backscatter with increasing SSC for SSC < 5 to 8 kg/m^3, and a decreasing backscatter amplitude with increasing SSC for larger SSCs. Such a relation was believed to be caused by some signal attenuation, linked to multiple scattering and associated sound absorption, in the sediment-laden flow (Downing et al., 1995; Guerrero et al., 2011; Ha et al., 2009). For comparison, the sediment-laden water sample

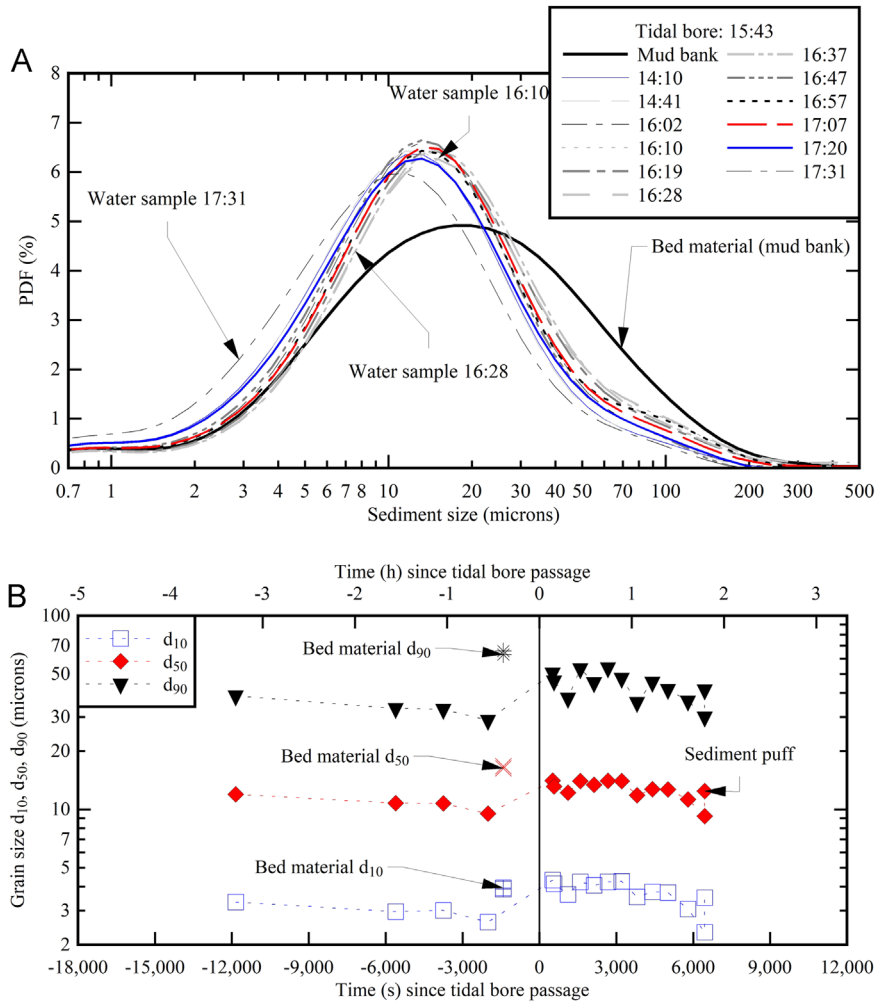

Fig. 4. Granulometry data for bed and suspended sediment samples collected in the Arcins Channel, Garonne River on 14 November 2016; (A) Probability distribution functions (PDFs) of the averaged volume fraction of sediment particle sizes - Thick line: sediment bed material; Thin lines: suspended sediment - The time of tidal bore passage is given in legend; and (B) Time variations of characteristic suspended sediment grain sizes (d_{10}, d_{50} and d_{90}) as functions of the relative tidal bore passage time (where d_x is the diameter of a sediment particle for which x percent of the particles are finer).

results are shown in Fig. 6, presenting the SSC as a function of the time of passage of the tidal bore. The water sample data sets showed a low SSC prior to the tidal bore: SSC $\approx$ 3–7 kg/m^3. After the bore, the SSCs were substantially higher, with SSC up to 100 kg/m^3 on 15 November 2016 about 7 minutes after the bore passage. As a result, the relation between SSC and backscatter amplitude was assumed to be monotically increasing prior to the tidal bore:

$$SSC = \frac{-305.28}{1 - 1.1492 \times 10^5 \times e^{-0.0523 \times Ampl}} \quad SSC < 9 \ kg/m^3 \tag{3}$$

where the backscatter amplitude (Ampl) is in counts. During and after the passage of the tidal bore, the relation between SSC and backscatter amplitude was assumed to be monotically decreasing:

$$SSC = 6 + \sqrt{-5.366 \times 10^3 \times Ln\left(\frac{Ampl}{160}\right)} \quad SSC > 10 \ kg/m^3 \tag{4}$$

Eqs. 3 and 4 are compared to the calibration data in Fig. 5. These equation were applied to the field data sets before and after the bore passage, respectively.

Rheometry data for the bed materials showed differences between loading and un-loading that were consistent with a non-Newtonian thixotropic behaviour. The basic outputs included the apparent yield stress, τ_c, and effective viscosity, μ, calculated based upon the unloading data, in line with earlier thixotropic material studies (Keevil et al., 2015; Reungoat et al., 2017a; Roussel et al., 2004). For the current data set, the apparent viscosity and yield stress were respectively 9.5 Pa s and 16 Pa on average. The results are compared to previous data in Table 2, showing quantitatively consistent findings in the Arcins Channel.

3. Results

3.1. Basic observations

On both days, the bore formation occurred at the downstream end of the Arcins Channel (Fig. 1A & Digital Appendix movies 00011.MTS and 00015.MTS). The bore front extended across the entire breadth of the channel, initially as a breaking bore because of sand bars. The tidal bore advanced upstream and its shape evolved in response to changes in bed topography (Digital Appendix movies 00011.MTS and 00015.MTS). The tidal bore was typically undular across most of the channel width, although some breaking was observed next to the river bank, as illustrated in Fig. 1A and Digital Appendix movie 00078b.AVI. At the sampling location, the water surface rose rapidly during the bore passage (Fig. 7A). On 15 November 2016, a surfer surfed the front of the bore for the full length of the channel (Digital Appendix movie 00078b.AVI). On each day, the tidal bore front was followed by secondary undulations, called whelps, with a wave period about 0.8–1 s. A period of strong

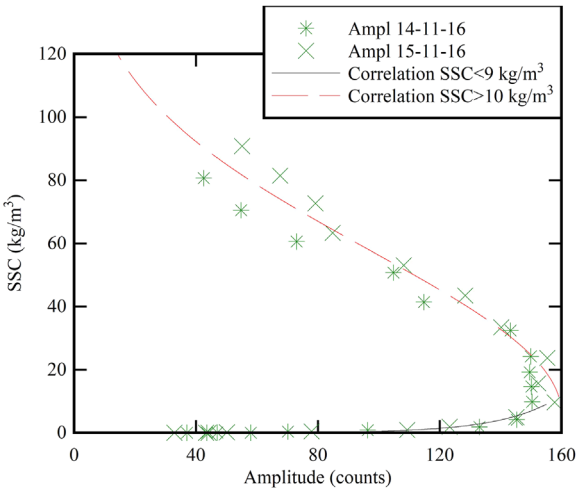

Fig. 5. Relation between suspended sediment concentration (SSC) and ADV acoustic signal amplitude (Ampl) for dilute solutions of sediment samples collected in the Arcins Channel, Garonne River in November 2016 - Legend indicates calibration data date.

pseudo-chaotic waves was further observed about 30 s after the bore front passage, which lasted for 1 to 1.5 minutes. The typical wave period, during this chaotic wave motion, was about 1.33 s and 1.16 s on 14 and 15 November 2016, respectively. The occurrence of such strong pseudo-chaotic waves could indicate some interplay between underwater bed form motion and the turbulent flow field (Chanson, 2000; Kennedy, 1963).

The strength of a tidal bore is defined in terms its Froude number, Fr_1:

$$Fr_1 = \frac{V_1 + U}{\sqrt{g \times \frac{A_1}{B_1}}} \quad (5)$$

where V_1 is the late ebb tide velocity positive downstream, U is the bore celerity positive upstream, g is the gravity acceleration, A_1 is the initial flow cross-sectional area, and B_1 is the initial free-surface width. The Froude number was 1.10 and 1.07 on 14 and 15 November 2016, respectively, for which an undular bore may be expected (Peregrine, 1966). On each day, the water elevation dropped gradually during the ebb tide (Fig. 7A). When the tidal bore advanced rapidly along the channel, its passage led to a rapid rise of the water elevation. This was followed by free-surface undulations and then a short pseudo-chaotic whelp motion (Fig. 7B). The water elevation increased rapidly with time during the entire flood tide. Fig. 7 shows a data set. All free-surface data are shown in Fig. 7A and compared to the water elevation records in Bordeaux. Fig. 7B shows a detailed data set about the tidal bore passage.

Table 2
Rheometry test average results (yield stress τ_c, apparent viscosity μ) of Garonne River bed sediment samples collected in the Arcins Channel (France) at end of ebb tide prior to tidal bore passage - Comparison between 2016 and earlier studies at the same site (Chanson et al., 2011; Keevil et al., 2015; Reungoat et al., 2014 ,2017a).

Bed sediment sample collection date	τ_c Pa	μ Pa.s	Number of tests
15 November 2016	13.05	7.80	5
14 November 2016	19.01	11.23	5
27 October 2015	11.35	3.61	2
1 September 2015	14.01	9.25	5
31 August 2015	12.40	8.92	5
30 August 2015	10.29	7.33	5
29 August 2015	11.09	7.17	2
19 October 2013	5.93	4.48	6
8 June 2012	37.1	9.1	3
7 June 2012	173	26.8	2
11 September 2010	55.5	48.8	2

The bore passage significantly impacted the velocity field in the channel, as illustrated in Fig., 7B. Fig. 7B shows a typical data set in terms of instantaneous water depth and velocity data. Herein the longitudinal velocity component, V_x, is positive downstream, the transverse velocity component, V_y, is positive towards the Arcins Island, and the vertical velocity, V_z, is positive upwards. All observations showed a very-rapid flow deceleration during the bore front passage, immediately followed by a change in flow direction. Large and rapid fluctuations of all velocity components were recorded during the early flood tide. With the bore passage, maximum flow decelerations ranged from -0.81 m/s^2 to less than -0.56 m/s^2, comparable to past field observations.

The early flood tidal flow was very energetic. About 20 s after the bore, the longitudinal turbulence intensity $v_x'/|V_x|$ was about 8–9%, where $|V_x|$ is the mean velocity magnitude. At 100 s after the bore front, a strong pseudo-chaotic free-surface wavy motion was observed, with large oscillations of both horizontal and vertical velocity components of periods slightly less than 1 s. These oscillations are seen in Fig. 7B for 56,640 s $<$ t $<$ 56,690 s. The oscillations are believed to be closely linked to free-surface curvature and its induced vertical motion, which might indicate active bed form motion (Charru et al., 2011; Kennedy, 1963). About one hour after the bore passage, the flood flow was still very turbulent, with the longitudinal turbulence intensity $v_x'/|V_x|$ about 10%. The horizontal turbulence ratio v_y'/v_x' was about 2/3, while the vertical turbulence ratio v_z'/v_x' was about 0.5.

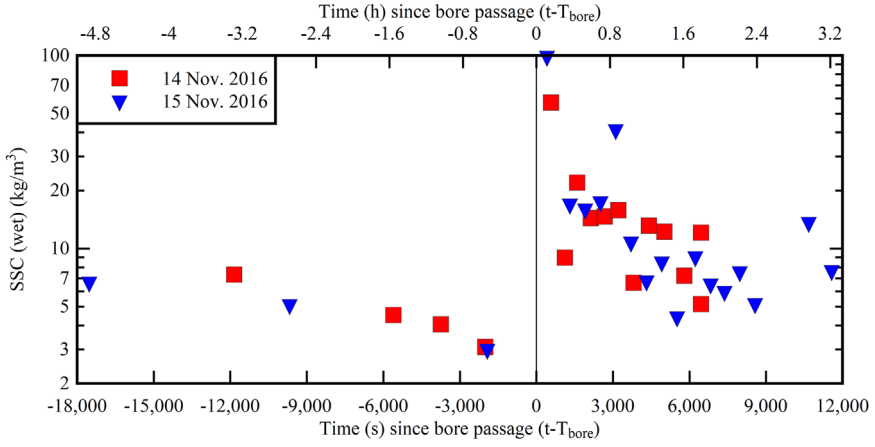

Fig. 6. Suspended sediment concentration of sediment-laden water samples collected at Arcins on 14 and 15 November 2016 as a function of the time relative to the time of passage of a tidal bore on the day of collection.

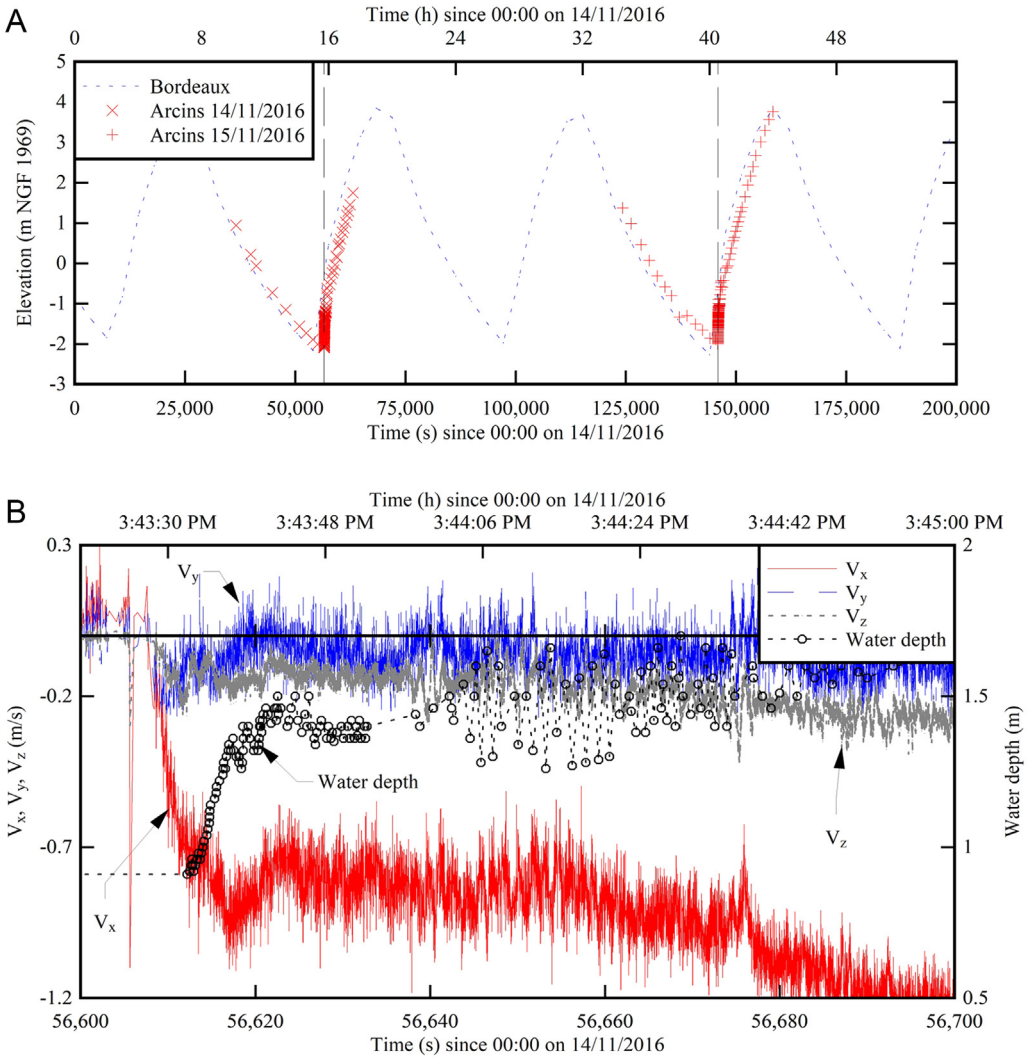

Fig. 7. Time variations of the water elevation in the Arcins Channel during the tidal bore field observations on 14 and 15 November 2016 - Note that the time is expressed since 00:00 on 14 November 2016; (A) Measured water elevations in the Arcins Channel and at Bordeaux (44 °52'N, 0 °33'W) (Data: Vigicrue, Ministère de l'Environnement et du Développement Durable) on 14 and 15 November 2016 - The Bordeaux data were collected 8.8 km downstream - Vertical dashed lines: tidal bore passage at sampling site; and (B) Detailed observations of water depth and instantaneous velocity components as functions of time during the Arcins Channel tidal bore on 14 November 2016 about the tidal bore passage.

The current observations were consistent with earlier field observations, in particular in terms of flow deceleration during bore passage and very-early flood tide velocity fluctuation levels (Chanson et al., 2011; Furgerot et al., 2016; Reungoat et al., 2014, 2017a; Simpson et al., 2004; Wolanski et al., 2004). The current data further indicated some turbulence anisotropy during the entire flood tide motion, including the tidal bore passage and strong wave motion.

3.2. Suspended sediment characteristics

The SSC estimates, calculated from the acoustic backscatter signal data, yielded long continuous high-frequency (200 Hz) records of instantaneous SSCs, as well as instantaneous suspended sediment flux per unit area, $q_s = SSC \times V_x$. All the data showed low SSC levels during the ebb tide, with very low SSC levels at end of the ebb tide. The bore passage was associated with a drastic increase in SSC level, together with fast and large fluctuations in SSC estimates. Immediately behind the bore front, the water surface became dark brown and SSCs in excess of 100 kg/m^3 were recorded for several minutes. On both days, maximum SSC estimates were observed about 7–8 min after the bore passage, with maximum instantaneous SSC estimates up to 150 kg/m^3 (Table 3), compared to maximum water sample SSC of 100 kg/m^3. The SSC levels tended to decrease, about 20 min after the bore passage. A key feature was the very large fluctuations in SSC estimates, with standard deviations SSC' $\approx$ 10 kg/m^3 about 20 s after the bore (Table 3). Typical results are shown in Fig. 8. Current results showed a strong link between turbulent bursting events and suspended sediment concentrations, as previously reported in the field (Amirshahi et al., 2018; Leng et al., 2018).

Some agreement between SSC estimates and water sample SSCs was observed, although the latter were collected very close to the water surface. The data were also comparable to previous field data in the Garonne River and in other estuarine systems (Fan et al., 2012; Furgerot et al., 2016; Keevil et al., 2015). Table 3 summarises key results in the Garonne River tidal bore between 2012 and 2016.

On both 14 and 15 November 2016, the flood tide motion presented fascinating patches of sediment boils at the free surface. These likely corresponded to large scale turbulent structures, originating from the bed and bursting at the free surface. The boundaries of each sediment patch/boil were very well defined, and mixing occurred very slowly, as evidenced by the differences in water surface colours. These patches were advected upstream by the flood flow and their sizes would range from about 0.1 m to 10 m. On 14 November 2016,

Table 3
Suspended sediment concentration and suspended sediment flux estimates in the Arcins Channel immediately prior to, during and immediately after the tidal bore in 2012, 2013, 2015, and 2016.

Suspended sediment & flow properties	Date 7/6/12	19/10/13	29/8/15	30/8/15	31/8/15	1/9/15	27/10/15	14/11/16	15/11/16
Froude number Fr_1	1.02	1.27	1.18	1.34	1.70	1.38	1.33	1.10	1.07
Late ebb tide (T_{bore}-100 s)									
Initial water depth (m) ([1])	2.72	2.05	1.685	1.25	1.12	1.28	1.24	0.99	0.86
Initial $\overline{SSC}$ (kg/m^3) ([2])	34.1	2.4	0.4	1.6	***22.1***	0.3	0.7	0.08	0.02
Initial SSC' (kg/m^3)	2.01	–	0.67	2.94	***17.6***	***16.3***	0.66	0.077	0.013
Initial flux $\overline{q_s}$ (kg/m^2/s) ([2])	11.6	0.25	0.04	0.16	0.01	0	0.05	0.007	0.001
Very early flood tide (T_{bore}+20 s)									
$\overline{SSC}$ (kg/m^3) ([2])	32.8	25.9	57.9	64.7	54.9	49.8	54.0	84.9	90.7
SSC' (kg/m^3)	2.49	–	8.25	7.24	7.66	7.51	8.64	9.94	10.61
$\overline{q_s}$ (kg/m^2/s)	-15.15	-20.5	-47.4	-53.8	-45.1	-41.8	-44.0	-69.7	-69.4
q_s' (kg/m^2/s)	1.58	–	8.54	8.97	6.68	7.14	7.84	6.66	6.71
Flood tide									
SSC_{max} (kg/m^3) ([2])	47.5	59.3	128.9	93.0	130.5	107.1	94.9	130.4	149.6
Time after bore passage (s)	397	487	663	577	534	562	452	22.2	495
$(q_s)_{max}$ (kg/m^2/s)	***-33.1***	-73.4	-194.3	-152.0	-198.6	-131.1	-123.9	-193.3	-179.9
Time after bore passage (s)	***1,862***	457	616	248	534	529	134	519	386
Early flood tide ($T_{bore} < t < T_{bore}$+3600 s)									
$\overline{SSC}$ (kg/m^3) ([2])	31.7	31.55	68.0	38.5	35.6	40.5	25.9	42.5	46.7
$\int_{T_{bore}}^{T_{bore}+1hour} SSC \times V_x \times dt$ (kg/m^2)	-0.726×10^5	-0.800×10^5	-2.71×10^5	-1.50×10^5	-1.41×10^5	-1.38×10^5	-1.94×10^5	-1.54×10^5	-1.72×10^5

Notes: q_s': standard deviation of suspended sediment flux per unit area; SSC': standard deviation of suspended sediment concentration; ([1]): at survey staff; ([2]): ADV data; Grey shaded data: OBS data (5 s average); ***Bold italic data***: suspicious data; Data sets: , Keevil et al. (2015), Current study.

two water samples were collected within a minute, about 2 h after the tidal bore passage; one sample was taken in a patch of mud flocs, and the other outside this patch. In the turbulent patch of mud flocs, the SSC was more than twice the SSC outside of a mud floc boil: i.e. 12.1 kg/m^3 versus 5.15 kg/m^3 (Reungoat et al., 2017b).

4. Discussion

The propagation of a tidal bore is a highly unsteady process. A time-averaging would be physically meaningless during the rapid passage of an abrupt bore front, i.e. the rapidly decelerating phase of the flow. Hence this short period was ignored, as indicated by some shading in Fig. 9. (The start of shaded area marked the arrival of the bore front, and the end of the shaded area corresponded to the end of the rapidly decelerating flow phase.) In this section, only the quasi-steady flows prior to and after the passage of the bore front are discussed. A statistical summary is provided in Table 4, for three characteristic periods: i.e. ebb tide ($t < T_{bore}$), early flood tide ($0 < t\text{-}T_{bore} < 6{,}000$ s) and late flood tide ($t\text{-}T_{bore} > 6{,}000$ s) where T_{bore} is the time of passage of the bore front.

On both days, the longitudinal velocity decreased gradually with time before the bore arrival. After the rapid deceleration during the bore passage, the mean longitudinal velocity became negative, indicating a flow reversal (Fig. 9A). The maximum amplitude of negative velocity was reached at the end of the deceleration phase and was equal to -1 m/s on both days. The longitudinal velocity component data showed large fluctuations with long irregular periods after the bore passage, an increasing magnitude and a negative sign for the first 6,000 s following the bore passage (Fig. 9B). Beyond 6,000 s after the bore, the average longitudinal velocity magnitude decreased with time. The decrease was relatively gentle with lesser fluctuations. All the velocity components showed the largest fluctuations during the early flood tide phase (Fig. 9B). The integral time scale data indicated a marked increase in the turbulent time scales after the bore passage, for all velocity components on both days (Fig. 9C). In Fig. 9C, note the scale for the integral time scale: in ms with a logarithmic scale. On average, the integral time scale before the bore was about 0.3–0.4 s for all velocity components. After the bore passage, T_E increased to 0.6–1.6 s (Table 4). The time-variations of integral time showed relatively large fluctuations after the bore. The integral time scale of all velocity components decreased slightly 8,000 s after the bore front passage. Overall, the current data showed quantitatively similar results to previous studies done in the Arcins Channel (Reungoat et al., 2015), as well as in a small estuary with micro-tidal flow conditions (Trevethan et al., 2007, 2008).

The passage of the tidal bore caused a substantial increase in all six components of the Reynolds stress tensor. This is seen in the time-variations of mean shear stresses shown in Figs. 9D, 9E, and 9F. The maximum Reynolds stresses happened shortly after the passage of the bore, with maximum instantaneous Reynolds stress magnitudes in excess of 150 Pa. The average Reynolds stress magnitudes later decreased gradually during the early flood tide phase. During the late flood tide phase (Fig. 9), the Reynolds stress data showed a secondary peak, seen in all six components at about 10,450 s (2 h 54 min) after the first peak. The duration of this large shear stress event though was much longer than the first peak: e.g., 3,000 s compared to 920 s for the normal stress component v_xv_x. This (un-expected) increase in stress amplitudes during the later flood tide period was not caused by the extreme values/outliers of the data sets, and was also observed in terms of the median and quartile data. Two stress components were associated with the most marked secondary peaks: i.e. the normal stress v_xv_x and tangential stress v_xv_z (Figs. 9D and 9F). The observation would suggest that the phenomenon might be linked to some sedimentary process at the velocity sampling point, possibly causing a

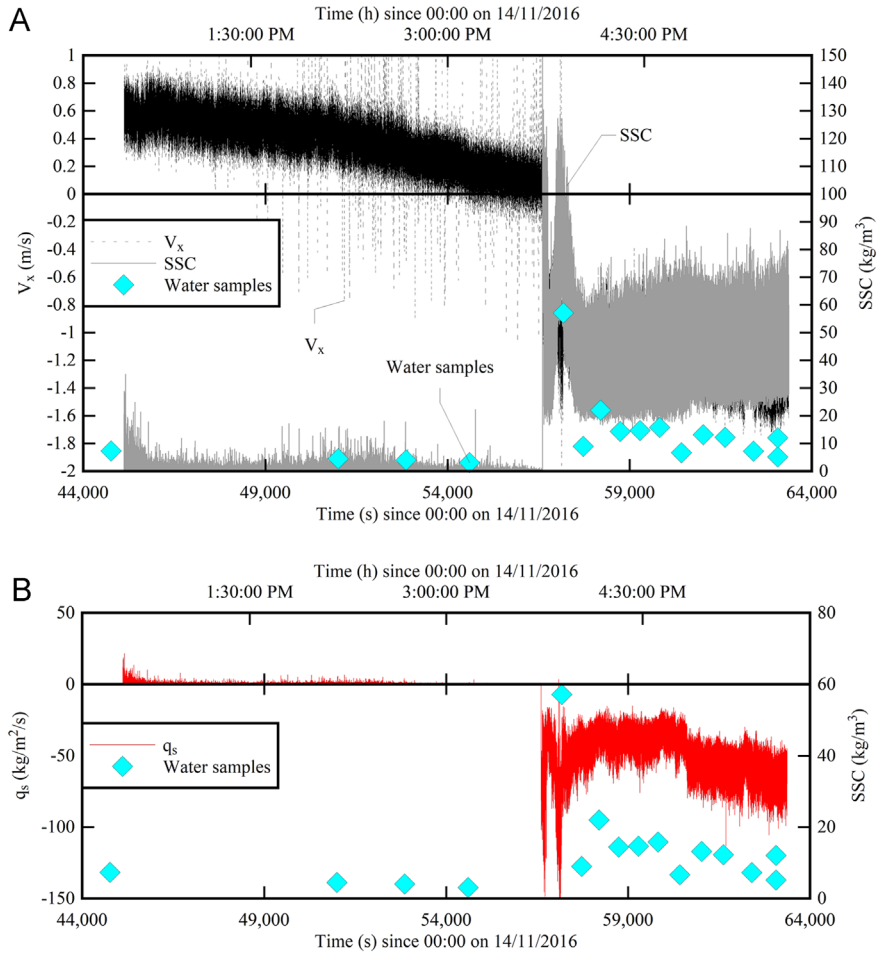

Fig. 8. Time variations of instantaneous suspended sediment concentration estimates and instantaneous suspended sediment flux per unit area on 14 November 2016 - Note that the time is expressed since 00:00 on 14 November 2016; (A) Instantaneous suspended sediment concentration data - Comparison with longitudinal velocity data and water sample SSC data; and (B) Instantaneous suspended sediment flux per unit area - Comparison with water sample SSC data.

change in shear stress between layers of fluid with suspended sediment bursting, or linked to some density stratification although it could be associated with wind waves.

The average SSC (i.e. $\overline{SSC}$) was very small during the late ebb tide before the bore. The mean SSC data showed two consecutive peaks immediately after the bore front passage (Fig. 9G). The second peak occurred typically within 380 s to 420 s after the first peak, with a higher magnitude. The SSC fluctuations, i.e. SSC', showed two peaks as well, with the second peak being lower in amplitude compared to the first peak in SSC'. The timing of the SSC fluctuation (i.e. SSC') peaks differed from those of the mean SSC data (i.e. $\overline{SSC}$). Namely, both peaks of SSC fluctuations happened slightly earlier than the two peaks in mean SSC. Both $\overline{SSC}$ and SSC' decreased significantly after the second peak. The SSC fluctuations remained relatively constant during the latter phase of flood tide, whereas the mean SSC data increased steadily with time during the late flood tide (Fig. 9G). The SSC integral time scale $T_{E,SSC}$ represented a characteristic time scale of turbid suspensions at the sampling point (Jackson, 1976) and it might be related to the suspended particle time scale (Chanson & Trevethan, 2011). The integral time scale, $T_{E,SSC}$, data showed a sharp increase as the bore front passed, followed by fluctuations with consecutive peaks as the secondary undulations and whelps propagated. The peaks in $T_{E,SSC}$ lasted for approximately 1,000 s on both 14 and 15 November 2016, before decreasing towards very small values, except for occasional jumps in data, during the latter phase of the flood tide. The average integral time scale during the early flood tide was around 1 s to 1.4 s. These time scales were consistent in terms of order of magnitude with the observations of integral time scales in velocity signals (Table 4). The fluctuations of the SSC integral time scale were more rapid compared to the fluctuations of mean SSC. In addition, the first peak in T_E occurred earlier than the first peak in mean SSC, indicating the possible existence of micro-turbulent structures which could be linked to the subsequent sediment erosion and upward sediment advection. The second highest peak in T_E happened prior to the second peak in SSC, however, with less strength.

The integral time scales for the three velocity components, $T_{E,x}$, $T_{E,y}$, and $T_{E,z}$ and for the suspended sediment concentration (SSC), $T_{E,SSC}$, are compared in Table 4. The ratio between the integral time scales of different velocity components were found to be $T_{E,y}/T_{E,x} \sim 0.2–0.7$ and $T_{E,z}/T_{E,x} \sim 0.2–1.3$, regardless of the tidal phase (ebb tide or flood tide). This indicated the three-dimensional nature and anisotropy of the flow before and after the immediate passage of the bore front. A comparison between turbulent and SSC integral time scales showed fascinating features (Table 4). The ratio of integral time scales of SSC to longitudinal velocity was on average $T_{E,SSC}/T_{E,x} \sim 0.16$ during the late ebb tide, compared to $T_{E,SSC}/T_{E,x} \sim 0.09$ during the late flood tide. Note that the two test days yielded different results. The ratio of integral time scales of SSC to velocity provides some quantitative information on the time scale of the suspended sediment process relative to the turbulent time scale. The latter is some indication of the lifespan of turbulent vortices (Bradshaw, 1971; Chanson, 2014). During the

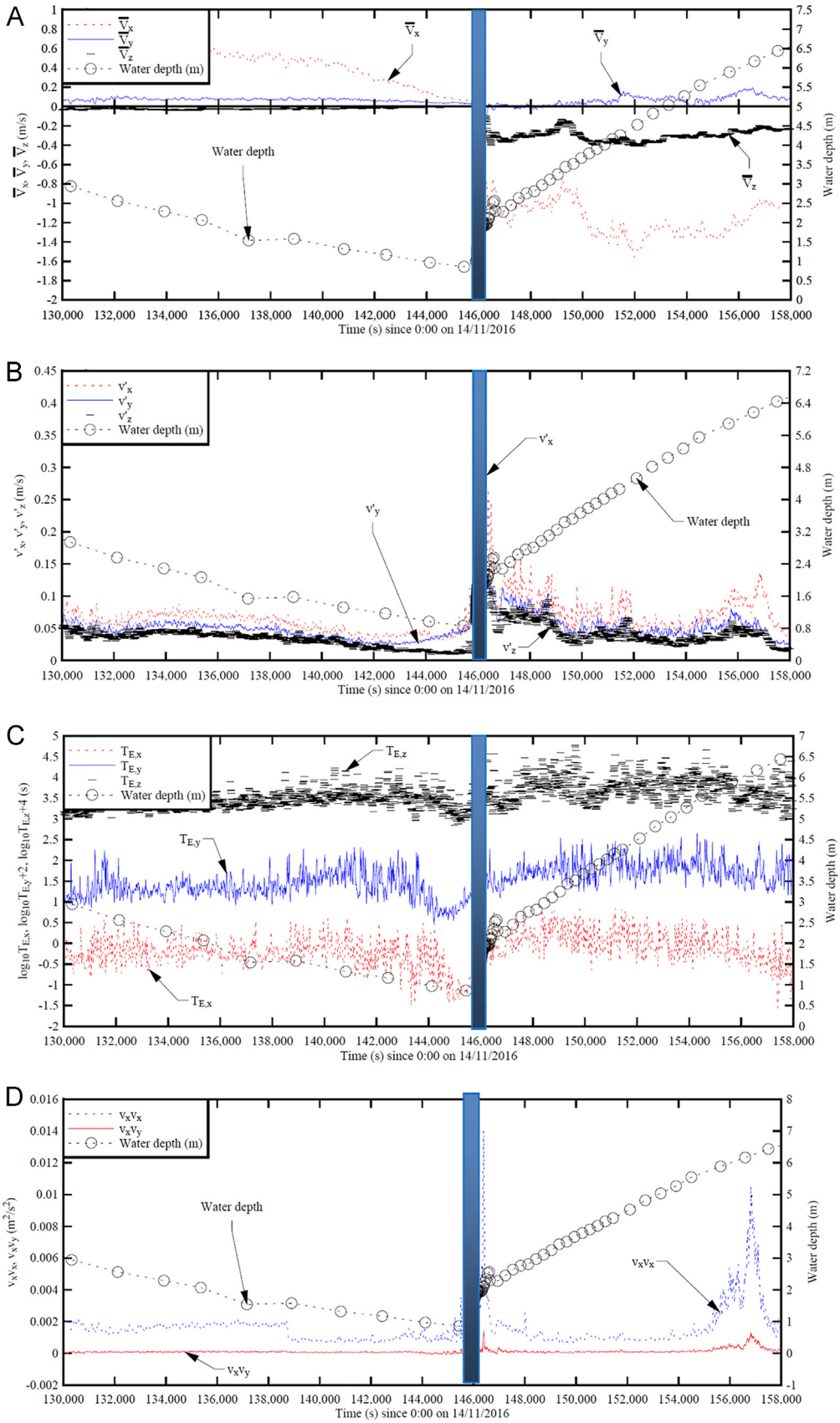

Fig. 9. Time-variations of average velocity components (V_x, V_y, V_z), velocity root mean square (RMS) (v_x', v_y', v_z'), integral time scales, average Reynolds stress tensor components, average SSC, SSC fluctuations, SSC integral time scale, in the Arcins Channel during the tidal bore on 15 November 2016 - Comparison with the water depth data - The shaded area corresponds to the rapidly=varied flow region about the tidal bore passage; (A) Average velocity components V_x, V_y and V_z;. (B) Velocity fluctuations v_x', v_y' and v_z'; (C) Integral time scales $T_{E,x}$, $T_{E,y}$ and $T_{E,z}$ - Note the logarithmic scale for the integral time scales (in ms); (D) Normal stress component v_x^2 and tangential stress component $v_x \times v_y$; (E) Normal stress component v_y^2 and tangential stress component $v_y \times v_z$; (F) Normal stress component v_z^2 and tangential stress component $v_x \times v_z$; and (G) Average SSC, standard deviation of SSC (SSC') and integral time scale T_E of SSC data - Note the logarithmic scale for the integral time scale data (in ms).

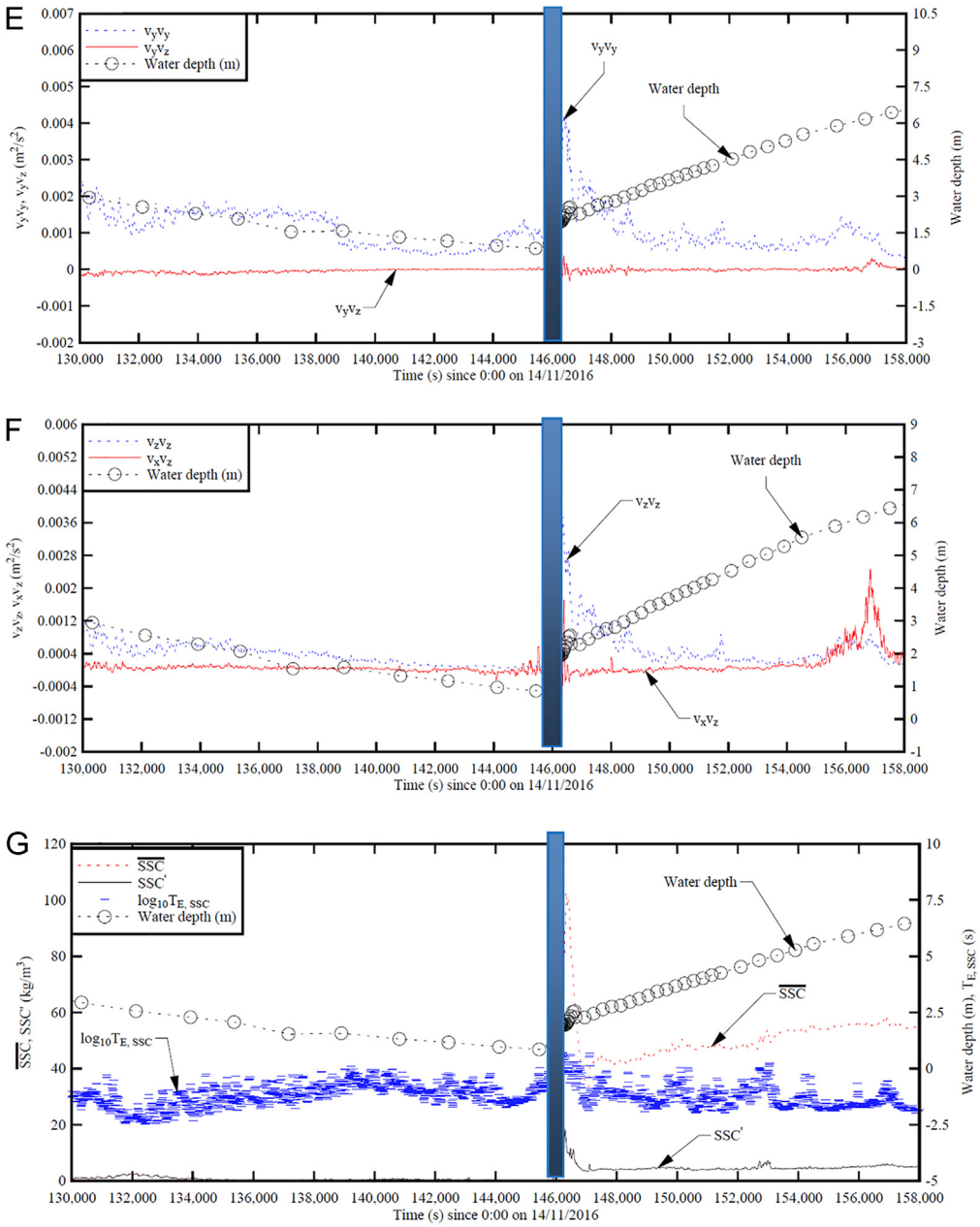

Fig. 9. *Continued.*

late ebb tide, the water flow was gradually-varied, pseudo-steady, and shallow. In contrast, the late ebb tide was a more energetic flow motion with a deeper and wider channel cross-section. While both integral time scales of SSC and velocity were substantially larger in the late flood tide, it is hypothesised that the larger increase in suspended sediment time scale was linked to the combination of large vortical structures, large amount of suspension and the fine texture of sediment suspension. The current findings differed quantitatively from data in a micro-tidal estuary (Chanson et al., 2007; Chanson & Trevethan, 2011). They, however, agreed qualitatively and showed substantially different time scales for the turbulent velocities and suspended sediment concentrations. This finding supported the theoretical development of Toorman (2008), and tended to suggest that the sediment suspension and suspended sediment fluxes were not dominated by the turbulent processes in the Arcins Channel. The substantial difference in time scales for turbulent mixing and sediment mixing implies that there were interactions and modulation between the two mixing processes, including particle trapping in coherent structures, reduced/enhanced particle settling and turbulence modulation (Nielsen, 2009; Tooby et al., 1977), while high suspended sediment concentration could lead to non-Newtonian fluid flow behaviour (Brown & Chanson, 2012; Keevil et al., 2015).

Overall the current results imply that (a) the turbulent flow motion was anisotropic and three-dimensional, and (b) the turbulent and sediment mixing processes exhibited significantly different time scales in the Arcins Channel. While the latter may be understandable during the bore passage, a basic question remains about what drives the turbulence during the flood flow motion.

5. Conclusions

New field measurements in the tidal bore of the Garonne River in the Arcins Channel were done on 14–15 November 2016. The investigation focused on long, continuous, high-frequency records

Table 4
Summary of turbulent and sediment characteristics during an ebb and flood tide flow in the tidal-bore affected Garonne River on 14 and 15 November 2016 in the Arcins Channel.

Field study date	Tidal period	v_x' (m/s)	SSC' (kg/m^3)	$T_{E,x}$ (s)	v_y'/v_x'	v_z'/v_x'	$T_{E,y}/T_{E,x}$	$T_{E,z}/T_{E,x}$	$T_{E,ssc}/T_{E,x}$
(1)	(2)	(3)	(4)	(5)	(6)	(7)	(8)	(9)	(10)
14 Nov. 2016	Ebb tide	0.060	0.27	0.46	0.67	0.50	0.48	0.70	0.15
	Early flood tide (6,000 s after bore)	0.090	4.90	1.65	0.78	0.56	0.37	0.37	0.13
	Late flood tide	–	–	–	–	–	–	–	–
15 Nov. 2016	Ebb tide	0.060	0.70	0.71	0.67	0.83	0.42	0.41	0.17
	Early flood tide (6,000 s after bore)	0.100	5.12	1.84	0.70	0.60	0.36	0.41	0.17
	Late flood tide	0.070	4.99	0.91	0.71	0.43	0.85	0.71	0.09

Notes: SSC': standard deviation of suspended sediment concentration; $T_{E,x}$; integral time scale of longitudinal velocity; $T_{E,y}$; integral time scale of transverse velocity; $T_{E,z}$; integral time scale of vertical velocity; $T_{E,ssc}$; integral time scale of suspended sediment concentration; v_x': standard deviation of longitudinal velocity component; v_y': standard deviation of transverse velocity component; v_z': standard deviation of vertical velocity component; (–): data set too short to be statistically meaningful.

of instantaneous velocity and suspended sediment concentration (SSC) estimate for several hours during the ebb tide, tidal bore passage, and flood tide. The aim of the study was to comprehend the temporal evolution of suspended sediment properties during the flood tide, in a tidal bore affected estuarine zone.

The bore passage induced a major change in the channel hydrodynamics, linked to a rapid flow deceleration and flow reversal during the tidal bore. The flood tide was characterised by some very intense turbulent and sediment mixing, as demonstrated by large and rapid fluctuations of all velocity fluctuations and large SSCs. The SSC data showed maximum instantaneous SSC estimates larger than 100 kg/m^3 shortly after the bore passage. The maximum suspended sediment concentration, and maximum suspended sediment flux, occurred about 400–500 s after the tidal bore. The SSC estimate data showed a decreasing trend from 20 minutes (1,200 s) after the bore passage. The granulometry data showed larger grain sizes (d_{10}, d_{50}, d_{90}) of suspended sediment in water samples compared to sediment bed materials, with a broader distribution, shortly after the bore passage. The suspended sediment flux data indicated that the tidal bore generated a sudden sediment flux reversal and a marked increase in sediment flux magnitude.

The time variations of turbulent velocity, Reynolds shear stress, and suspended sediment properties showed large fluctuations throughout the entire data set. The results implied that the turbulent flow motion was anisotropic and three-dimensional. On both days, the peaks of SSC fluctuations (i.e. SSC') happened slightly earlier than the peaks in mean SSC (i.e. $\overline{SSC}$). The ratio of integral time scales of SSC to velocity in the x-directio was on average $T_{E,SSC}/T_{E,x} \sim 0.16$ during the late ebb tide, compared to $T_{E,SSC}/T_{E,x} \sim 0.09$ during the late flood tide. The results showed markedly different time scales for the turbulent velocities and suspended sediment concentrations.

Acknowledgements

The authors thank Professor Ioan Nistor (University of Ottawa) and Dr. Jeremy Bricker (Delft University of Technology) for their initial comments. They acknowledge the helpful inputs of Professor Pierre Lubin (University of Bordeaux). The authors also acknowledge the assistance of Patrice Benghiati and the permission to access and use the pontoon in the Bras d'Arcins. They thank all the people who participated to the field work, and without whom the study could not have been done. They also thank Antony Colas (Anglet, France) for a number of useful discussions and information. The authors acknowledge the financial assistance of the Agence Nationale de la Recherche (Projet MASCARET 10-BLAN-0911-01).

Competing interests

The authors have no competing interest.

Appendix A. Digital Appendix. Video movies

A number of video-movies were recorded during the field work on 14 and 15 November 2016. Three movies are included as part of the video data. Table A-1 list the details of each movie. The first two movies show the tidal bore about 400 m downstream of the sampling location, looking downstream at the incoming bore. The third movie was taken from a boat, about 1.5 m above the water surface, looking towards the left bank and Arcins Island. It features the end of the ebb tide, the passage of the bore filmed for nearly a minute, and the early flood tide.

Table A-1
Video files of Garonne River tidal bore propagation in the Arcins Channel.

Filename	Date	Camera	Description
00011.MTS	14 Nov. 2016	Sony HDR-PJ200	Looking downstream at incoming bore
00015.MTS	15 Nov. 2016	Sony HDR-PJ200	Looking downstream at incoming bore
00078b.AVI	15 Nov. 2016	Sony DSC-HX200V	Late ebb and early flood tide, viewed from a boat, with camera about 1.5 m above water level. Bore front seen from 0:31 to 1:29, with surfer surfing the bore along the left bank

Appendix B. Supplementary material

Supplementary data associated with this article can be found in the online version at https://doi.org/10.1016/j.ijsrc.2019.03.003.

References

Amirshahi, S. M., Kwoll, E., & Winter, C. (2018). Near bed suspended sediment flux by single turbulent events. *Continental Shelf Research*, *152*, 76–86. https://doi.org/10.1016/j.csr.2017.11.005.

Bartsch-Winkler, S., & Lynch, D. K. (1988). Catalog of worldwide tidal bore occurrences and characteristics. *US Geological Survey Circular*(1022).
Bradshaw, P. (1971). *An introduction to turbulence and its measurement*. Oxford, UK: Pergamon Press.
Brown, R., & Chanson, H. (2012). Suspended sediment properties and suspended sediment flux estimates in an urban environment during a major flood event. *Water Resources Research*, *48*, W11523. https://doi.org/10.1029/2012WR012381.
Chanson, H. (2000). Boundary shear stress measurements in undular flows: Application to standing wave bed forms. *Water Resources Research*, *36*(10), 3063–3076. https://doi.org/10.1029/2000WR900154.
Chanson, H. (2011). *Tidal bores, aegir, eagre, mascaret, pororoca: Theory and observations*. Singapore: World Scientific.
Chanson, H. (2014). *Applied hydrodynamics: An introduction*. Leiden, The Netherlands: CRC Press, Taylor & Francis Group.
Chanson, H., Reungoat, D., Simon, B., & Lubin, P. (2011). High-frequency turbulence and suspended sediment concentration measurements in the Garonne River tidal bore. *Estuarine Coastal and Shelf Science*, *95*(2–3), 298–306. https://doi.org/10.1016/j.ecss.2011.09.012.
Chanson, H., Takeuchi, M., & Trevethan, M. (2007). High-frequency suspended sediment flux measurements in a small estuary. In M. Sommerfield (Ed.), In Proceedings of the 6th International Conference on Multiphase Flow ICMF 2007, Leipzig, Germany, July 9–13, Session 7, Paper No. S7_Mon_C_S7_Mon_C_5, 12 pages (CD-ROM).
Chanson, H., & Toi, Y. H. (2015). Physical modelling of breaking tidal bores: Comparison with prototype data. *Journal of Hydraulic Research*, *53*(2), 264–273. https://doi.org/10.1080/00221686.2014.989458.
Chanson, H., & Trevethan, M. (2011). Vertical mixing in the fully developed turbulent layer of sediment-laden open-channel flow. Discussion. *Journal of Hydraulic Engineering*, *137*(9), 1095–1097. https://doi.org/10.1061/(ASCE)HY.1943-7900.0000218.
Charru, F., Andreotti, B., & Claudin, P. (2011). Sand ripples and dunes. *Annual Review of Fluid Mechanics*, *45*, 469–493.
Downing, A., Thorne, P. D., & Vincent, C. E. (1995). Backscattering from a suspension in the near field of a piston transducer. *Journal of Acoustical Society of America*, *97*(3), 1614–1620.
Fan, D. D., Cai, G. F., Wu, Y. J., Zhang, Y. W., & Gao, L. (2012). Sedimentation processes and sedimentary characteristics of the north bank of the Qiantang Estuary. *Chinese Science Bulletin*, *57*(13), 1578–1589. https://doi.org/10.1007/s11434-012-4993-6.
Fan, D., Tu, J., Shang, S., & Cai, G. (2014). Characteristics of tidal-bore deposits and facies associations in the Qiantang Estuary, China. *Marine Geology*, *348*, 1–14. https://doi.org/10.1016/j.margeo.2013.11.012.
Furgerot, L. (2014). Propriétés hydrodynamiques du mascaret et de son influence sur la dynamique sédimentaire. Une approche couplée en canal et in situ (estuaire de la Sée, Baie du Mont Saint Michel). Ph.D. dissertation, University of Caen Basse-Normandie, France, Spécialité: Terre Solide et Enveloppes Superficielles. (*In French*)
Furgerot, L., Mouaze, D., Tessier, B., Perez, L., Haquin, S., Weill, P., & Crave, A. (2016). Sediment transport induced by tidal bores. An estimation from suspended matter measurements in the Sée River (Mont-Saint-Michel Bay, northwestern France). *Comptes Rendus Géoscience*, *348*(6), 432–441. https://doi.org/10.1016/j.crte.2015.09.004.
Graf, W. H. (1971). *Hydraulics of sediment transport*. New York, USA: McGraw-Hill.
Greb, S. F., & Archer, A. W. (2007). Soft-sediment deformation produced by tides in a Meizoseismic area, Turnagain Arm, Alaska. *Geology*, *35*(5), 435–438.
Guerrero, M., Szupiany, R. N., & Amsler, M. (2011). Comparison of acoustic backscattering techniques for suspended sediments investigation. *Flow Measurement Instrumentation*, *22*, 392–401.
Ha, H. K., Hsu, W. Y., Maa, J. P. Y., Shao, Y. Y., & Holland, C. W. (2009). Using ADV backscatter strength for measuring suspended cohesive sediment concentration. *Continental Shelf Research*, *29*, 1310–1316.
Jackson, R. G. (1976). Sedimentological and fluid-dynamic implications of the turbulent bursting phenomenon in geophysical flows. *Journal of Fluid Mechanics*, *77*(3), 531–560.
Julien, P. Y. (1995). *Erosion and sedimentation*. Cambridge, UK: Cambridge University Press.
Keevil, C. E., Chanson, H., & Reungoat, D. (2015). Fluid flow and sediment entrainment in the Garonne River bore and tidal bore collision. *Earth Surface Processes and Landforms*, *40*(12), 1574–1586. https://doi.org/10.1002/esp.3735.
Kennedy, J. F. (1963). The mechanics of dunes and antidunes in erodible-bed channels. *Journal of Fluid Mechanics*, *16*(4), 521–544 (& 2 plates).
Kjerfve, B., & Ferreira, H. O. (1993). Tidal bores: First ever measurements. *Ciência e Cultura*, *45*(2), 135–138.
Larracey, E. W. (1985). *The Chocolate River. A story of the Petitcodiac River from the beginning of habitation in the late 1600's until the building of the causeway at Moncton*. Hantsport NS, Canada: Lancelot Press.
Leng, X., Chanson, H., & Reungoat, D. (2018). Turbulence and turbulent flux events in tidal bores: Case study of the undular tidal bore of the Garonne River. *Environmental Fluid Mechanics*, *18*(4), 807–828. https://doi.org/10.1007/s10652-017-9561-9.
Lighthill, J. (1978). *Waves in fluids*. Cambridge, UK: Cambridge University Press.
Nielsen, P. (2009). *Coastal and estuarine processes*, 29. Singapore: World Scientific, Advanced Series on Ocean Engineering.
Peregrine, D. H. (1966). Calculations of the development of an undular bore. *Journal of Fluid Mechanics*, *25*, 321–330.
Piquet, J. (1999). *Turbulent flows. Models and physics*. Berlin, Germany: Springer.
Reungoat, D., Chanson, H., & Caplain, B. (2014). Sediment processes and flow reversal in the undular tidal bore of the Garonne River (France). *Environmental Fluid Mechanics*, *14*(3), 591–616. https://doi.org/10.1007/s10652-013-9319-y.
Reungoat, D., Chanson, H., & Keevil, C. E. (2015). Field measurements of unsteady turbulence in a tidal bore: The Garonne River in October 2013. *Journal of Hydraulic Research*, *53*(3), 291–301. https://doi.org/10.1080/00221686.2015.1021717.
Reungoat, D., Leng, X., & Chanson, H. (2017a). Successive impact of tidal bores on sedimentary processes: Arcins channel, Garonne River. *Estuarine Coastal and Shelf Science*, *188*, 163–173. https://doi.org/10.1016/j.ecss.2017.02.025.
Reungoat, D., Leng, X., & Chanson, H. (2017b). Suspended sediment processes in the Garonne River tidal bore: Arcins Channel on 14-15 November 2016. Hydraulic Model Report No. CH108/17, School of Civil Engineering, The University of Queensland, Brisbane, Australia.
Roussel, N., Le Roy, R., & Coussot, P. (2004). Thixotropy modelling at local and macroscopic scales. *Journal of Non-Newtonian Fluid Mechanics*, *117*(2-3), 85–95.
Simpson, J. H., Fisher, N. R., & Wiles, P. (2004). Reynolds stress and TKE production in an estuary with a tidal bore. *Estuarine, Coastal and Shelf Science*, *60*(4), 619–627.
Tooby, P. F., Wick, G. L., & Isaacs, J. D. (1977). The motion of a small sphere in a rotating velocity field: A possible mechanism for suspending particles in turbulence. *Journal of Geophysical Research*, *82*(15), 2096–2100.
Toorman, E. A. (2008). Vertical mixing in the fully developed turbulent layer of sediment-laden open-channel flow. *Journal of Hydraulic Engineering*, *134*(9), 1225–1235. https://doi.org/10.1061/(ASCE)0733-9429(2008)134:9(1225).
Trevethan, M., Chanson, H., & Brown, R. (2008). Turbulent measurements in a small subtropical estuary with semi-diurnal tides. *Journal of Hydraulic Engineering*, *134*(11), 1665–1670. https://doi.org/10.1061/(ASCE)0733-9429(2008)134:11(1665).
Trevethan, M., Chanson, H., & Takeuchi, M. (2007). Continuous high-frequency turbulence and sediment concentration measurements in an upper estuary. *Estuarine Coastal and Shelf Science*, *73*(1–2), 341–350. https://doi.org/10.1016/j.ecss.2007.01.014.
Tricker, R. A. R. (1965). *Bores, breakers, waves and wakes*. New York, USA: American Elsevier Publishing Company.
Wolanski, E., Williams, D., Spagnol, S., & Chanson, H. (2004). Undular tidal bore dynamics in the Daly Estuary, Northern Australia. *Estuarine, Coastal and Shelf Science*, *60*(4), 629–636.